

# Semantic Foggy Scene Understanding with Synthetic Data

Christos Sakaridis · Dengxin Dai · Luc Van Gool

Received: date / Accepted: date

**Abstract** This work addresses the problem of semantic foggy scene understanding (SFSU). Although extensive research has been performed on image dehazing and on semantic scene understanding with weather-clear images, little attention has been paid to SFSU. Due to the difficulty of collecting and annotating foggy images, we choose to generate synthetic fog on real images that depict weather-clear outdoor scenes, and then leverage these synthetic data for SFSU by employing state-of-the-art convolutional neural networks (CNN). In particular, a complete pipeline to generate synthetic fog on real, weather-clear images using incomplete depth information is developed. We apply our fog synthesis on the Cityscapes dataset and generate *Foggy Cityscapes* with 20550 images. SFSU is tackled in two fashions: 1) with typical supervised learning, and 2) with a novel semi-supervised learning, which combines 1) with an unsupervised supervision transfer from weather-clear images to their synthetic foggy counterparts. In addition, this work carefully studies the usefulness of image dehazing for SFSU. For evaluation, we present *Foggy Driving*, a dataset with 101 real-world images depicting foggy driving scenes, which come with ground truth annotations for semantic segmentation and object detection. Extensive experiments show that 1) supervised learning with our synthetic data significantly improves the performance of state-of-the-art CNN for SFSU on *Foggy Driving*; 2) our semi-supervised learning strategy further improves performance; and 3) image dehazing marginally benefits SFSU with our learning strategy. The datasets, models

and code will be made publicly available to encourage further research in this direction.

**Keywords** Foggy scene understanding · Semantic segmentation · Object detection · Depth denoising and completion · Dehazing · Supervision transfer

## 1 Introduction

Camera sensors and accompanying vision algorithms are widely used for surveillance [9], remote sensing [16], and automated cars [31], and their deployment keeps expanding. While these sensors and algorithms are constantly getting better, they are mainly designed to operate on weather-clear images and videos [41]. As known, in any outdoor application such as autonomous driving and mobile mapping, it is hard to escape from “bad” weather. Thus, computer vision systems are highly expected to also function under adverse weather conditions. This work focuses on the condition of fog.

Fog degrades visibility of a scene significantly [42, 55]. This causes problems not only to human observers, but also to computer vision algorithms. During the past years, a large body of research has been conducted on image defogging (dehazing) to increase scene visibility [27, 43, 62]. Meanwhile, marked progress has been made in semantic scene understanding with weather-clear images and videos [14, 46, 63]. However, semantic understanding of foggy scenes has received little attention so far, despite its importance in outdoor applications. For instance, an automated car requires a robust detection of road lanes, traffic lights, and other traffic agents not only in a modest weather condition but also in the presence of fog. This work investigates the problem of semantic foggy scene understanding (SFSU).

C. Sakaridis · D. Dai · L. Van Gool  
ETH Zürich, Zurich, Switzerland

L. Van Gool  
KU Leuven, Leuven, Belgium

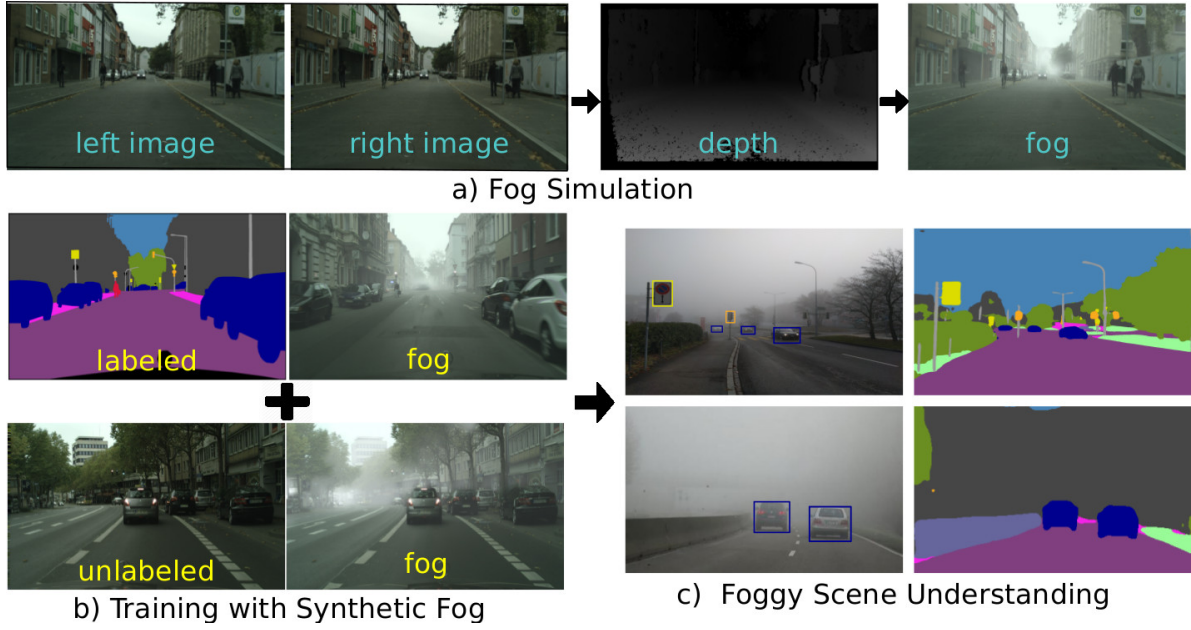


**Fig. 1** The pipeline of semantic foggy scene understanding with synthetic data: from a) fog simulation on real outdoor scenes, to b) training with pairs of synthetic foggy images and semantic annotations as well as pairs of foggy images and weather-clear images, and c) scene understanding of real foggy scenes. This figure is seen better on a screen

High-level semantic scene understanding tasks are usually tackled with the strategy of learning with large amount of annotations of real images [14, 51]. However, the difficulty of collecting and annotating images for unusual weather conditions such as fog renders this standard protocol problematic. To overcome this problem, we depart from this traditional paradigm and propose another route in this paper; we choose to generate synthetic fog into real images that contain weather-clear outdoor scenes, and then leverage these synthetic foggy images for SFSU.

Given the fact that large-scale annotated data are available for weather-clear images [14, 18, 22, 51], we in this work present an automatic pipeline to generate synthetic yet high-quality fog on such datasets. Our fog simulation uses the standard optical model for daytime fog [36], which has been used extensively in image dehazing, to overlay existing weather-clear images with synthetic fog in a physically sound way, simulating the underlying mechanism of foggy image formation. We leverage our fog simulation pipeline to create the *Foggy Cityscapes* dataset by adding fog to urban scenes from the Cityscapes dataset [14], leading to 550 carefully refined high-quality synthetic foggy images with fine semantic annotations inherited directly from Cityscapes, plus an additional 20000 synthetic foggy images. The resulting “synthetic-fog” images are used to train two semantic segmentation models [39, 63] and an object detector [23] for foggy scenes. The models are trained in two fashions: 1) by the typical supervised learning us-

ing the 550 high-quality foggy images and 2) by a novel semi-supervised learning which combines 1) with an unsupervised supervision transfer from weather-clear images to their foggy counterparts of the same scenes using the additional 20000 foggy images. For evaluation purposes, we collect and annotate a new dataset, *Foggy Driving*, with 101 images of driving scenes in a presence of fog. See Figure 1 for the whole pipeline of our work. In addition, this work carefully studies the usefulness of three state-of-the-art image dehazing (defogging) methods in increasing visibility in real foggy outdoor scenes and helping SFSU.

The main contributions of the paper are: 1) an automatic and scalable pipeline to impose high-quality synthetic fog on real weather-clear images; 2) two new datasets, one synthetic and one real, to facilitate training and evaluation of models used in SFSU; 3) a new semi-supervised learning approach for SFSU; and 4) a detailed study of the benefit of image dehazing for visibility and semantic understanding of foggy scenes.

The rest of the paper is organized as follows. Section 2 presents the relevant work. Section 3 is devoted to our fog simulation pipeline, which is followed by Section 4 that introduces our two foggy datasets. Section 5 describes supervised learning with our synthetic foggy data and Section 6 extends the learning to a semi-supervised paradigm, where supervision is transferred from weather-clear images to their synthetic foggy counterparts. Finally, Section 5.2 is devoted to

studying the usefulness of image dehazing for SFSU and Section 7 concludes the paper.

## 2 Related Work

Our work is generally relevant to image defogging (dehazing), depth denoising and completion, foggy scene understanding, and synthetic visual data.

### 2.1 Image Defogging/Dehazing

Fog fades the color of observed objects and reduces their contrast. Extensive research has been conducted on image defogging (dehazing) to increase the visibility of foggy scenes. This ill-posed problem has been tackled from different perspectives. For instance, in contrast enhancement [42, 55] the rationale is that weather-clear images have higher contrast than images degraded by fog. Depth and statistics of natural images are exploited as priors as well [5, 19, 43]. Another line of work is based on the dark channel prior [27], with the empirically validated assumption that pixels of weather-clear images are very likely to have low values in some of the three color channels. Due to its importance in outdoor applications, methods have been developed for nighttime as well [38]. A fast dehazing approach has been developed in [57] towards real-time applications. Recent approaches also rely on trainable architectures [56], which have evolved to end-to-end models [47]. All these approaches have achieved great performance in increasing visibility. Our work is complementary and focuses on semantic understanding of foggy scenes.

### 2.2 Depth Denoising and Completion

Synthesizing a foggy image from its real, clear counterpart generally requires an accurate depth map. In previous works, the colorization approach of [37] has been used to inpaint depth maps of the *indoor* NYU Depth dataset [53]. Such inpainted depth maps have been used in state-of-the-art dehazing approaches such as [47] to generate training data in the form of synthetic indoor foggy images. On the contrary, our work considers real *outdoor* urban scenes from the Cityscapes dataset [14], which contains significantly more complex depth configurations than NYU Depth. Furthermore, the available depth information in Cityscapes is not provided by a depth sensor, but it is rather an estimate of the depth resulting from the application of a semiglobal matching stereo algorithm based on [30]. This depth

estimate usually contains a large amount of severe artifacts and large holes (cf. Figure 1), which render it inappropriate for direct use in fog simulation. There are several recent approaches that handle highly noisy and incomplete depth maps, including stereoscopic inpainting [61], spatio-temporal hole filling [11] and layer depth denoising and completion [52]. Our method builds on the framework of stereoscopic inpainting [61] which performs depth completion at the level of superpixels, and introduces a novel, theoretically grounded objective for the superpixel-matching optimization that is involved.

### 2.3 Foggy Scene Understanding

Semantic understanding of outdoor scenes is a crucial enabler for applications such as assisted or autonomous driving. Typical examples include road and lane detection [4], traffic light detection [32], car and pedestrian detection [22], and a dense, pixel-level segmentation of road scenes to most of the relevant semantic classes [8, 14]. While deep recognition networks have been developed [23, 39, 46, 63, 65] and large-scale datasets have been presented [14, 22], the research focus of these works is mainly on clear weather. There is also a large body of work on image understanding of foggy scenes. For instance, fog detection has been tackled for daytime [6, 7, 44], nighttime [20], and for scenarios where time is at premium [54]. Classification of scenes into foggy and fog-free has been tackled as well [45]. In addition, visibility estimation and analysis have been extensively studied for both daytime [26, 40, 59] and nighttime [21] in the context of assisted and autonomous driving. Among those, the closest work to ours is [59], in which synthetic fog are generated and foggy images are segmented to *free-space area* and *vertical objects*. Our work differs in that: 1) our semantic understanding task is more complex, with 19 semantic classes that are commonly involved in driving scenarios, 8 of which occur as distinct objects; 2) we tackle the problem with modern deep CNN for semantic segmentation [39, 63] and object detection [23], taking full advantage of the most recent advances in this field; and 3) we compile and will release a large-scale dataset of synthetic foggy images based on real scenes plus a dataset of real-world foggy scenes, both with dense pixel-level semantic annotations and bounding box annotations for objects.

### 2.4 Synthetic Visual Data

The leap of computer vision in recent years is largely attributed to the availability of large labeled datasets [14, 18, 51]. However, acquiring and annotating a dataset

of this scale for each new problem is not a scalable alternative. Thus, learning with synthetic data is becoming more attractive. We summarize some notable examples. Dosovitskiy *et al.* [17] use the renderings of a floating chair to train dense optical flow regression networks. Gupta *et al.* [24] impose text onto natural images to learn an end-to-end text detection system. Vázquez *et al.* [60] train pedestrian detectors with virtual data. In [48, 49], the authors leverage video game engines to render images along with dense semantic annotations that are subsequently used in combination with real data to improve semantic segmentation performance of modern CNN architectures on real scenes. Going one step further, [33] shows that for the task of vehicle detection, training a CNN model *only* on massive amounts of synthetic images can outperform the same model which is trained on large-scale real datasets like Cityscapes. By contrast, our work tackles semantic segmentation and object detection for real *foggy* urban scenes by generating synthetic images from existing *real* images with clear weather. One exceptionally interesting work worth mentioning here is the project “FOG” [12], in which the team developed a prototype of a small-scale fog chamber which is able to produce stable visibility levels and homogeneous fog to test driver reaction.

### 3 Fog Simulation on Real Outdoor Scenes

To simulate fog on input images that depict real scenes with clear weather, the standard approach is to model the effect of fog as a function that maps the radiance of the clear scene to the observed radiance at the camera sensor. Critically, this space-variant function is usually parameterized by the distance  $\ell$  of the scene from the camera, which equals the length of the path along which light has traveled and is directly related to depth. As a result, the pair of the clear image and its corresponding depth map forms the basis of our foggy image synthesis. In this section, we first detail the optical model which we use for fog and then present our complete pipeline for fog simulation, with emphasis on our denoising and completion of the input depth. Finally, we present some criteria for selecting suitable images to generate high-quality synthetic fog.

#### 3.1 Optical Model of Choice for Fog

In the image dehazing literature, various optical models have been used to model the effect of haze on the appearance of a scene. For instance, optical models tailored for nighttime haze removal have been proposed

in [38, 64], taking into account the space-variant lighting that characterizes most nighttime scenes. This variety of models is directly applicable to the case of fog as well, since the physical process for image formation in the presence of either haze or fog is essentially similar. For our synthesis of foggy images, we consider the standard optical model of [36], which is used extensively in the literature [19, 27, 47, 56, 57] and is formulated as

$$\mathbf{I}(\mathbf{x}) = \mathbf{R}(\mathbf{x})t(\mathbf{x}) + \mathbf{L}(1 - t(\mathbf{x})), \quad (1)$$

where  $\mathbf{I}(\mathbf{x})$  is the observed foggy image at pixel  $\mathbf{x}$ ,  $\mathbf{R}(\mathbf{x})$  is the clear scene radiance and  $\mathbf{L}$  is the atmospheric light. This model assumes the atmospheric light to be globally constant, which is generally valid only for *daytime* images. The transmission  $t(\mathbf{x})$  determines the amount of scene radiance that reaches the camera. In case of a *homogeneous* medium, transmission depends on the distance  $\ell(\mathbf{x})$  of the scene from the camera through

$$t(\mathbf{x}) = \exp(-\beta\ell(\mathbf{x})). \quad (2)$$

Parameter  $\beta$  is named attenuation coefficient and it effectively controls the thickness of fog: larger values of  $\beta$  mean thicker fog. The meteorological optical range (MOR), also known as visibility, is defined as the maximum distance from the camera for which  $t(\mathbf{x}) \geq 0.02$ , which implies that if (2) is valid, then  $\text{MOR} = 3.912/\beta$ . Fog decreases the MOR to less than 1 km by definition [1]. Therefore, the attenuation coefficient in homogeneous fog is by definition

$$\beta \geq 3.912 \times 10^{-3} \text{ m}^{-1}, \quad (3)$$

where the lower bound corresponds to the lightest fog configuration. In our fog simulation, the value that is used for  $\beta$  always obeys (3).

Model (1) provides a powerful basis for simulating fog on outdoor scenes with clear weather. Even though its assumption of homogeneous atmosphere is strong, it generates synthetic foggy images that can act as good proxies for real world foggy images where this assumption might not hold exactly, as long as it is provided with an *accurate* transmission map  $t$ . Straightforward extensions of (1) are used in [58] to simulate heterogeneous fog on synthetic scenes.

To sum up, the necessary inputs for fog simulation using (1) are a color image  $\mathbf{R}$  of the original clear scene, atmospheric light  $\mathbf{L}$  and a dense transmission map  $t$  defined at each pixel of  $\mathbf{R}$ . Our task is thus twofold:

1. estimation of  $t$ , and
2. estimation of  $\mathbf{L}$  from  $\mathbf{R}$ .



Step 2 is simple: we use the method proposed in [27] with the improvement of [56]. In the following, we focus on step 1 for the case of outdoor scenes with a noisy, incomplete estimate of depth serving as input.

### 3.2 Depth Denoising and Completion for Outdoor Scenes

The inputs that our method requires for generating an accurate transmission map  $t$  are:

- the original, weather-clear color image  $\mathbf{R}$  to add synthetic fog on, which constitutes the *left* image of a stereo pair,
- the *right* image  $\mathbf{Q}$  of the stereo pair,
- the intrinsic calibration parameters of the two cameras of the stereo pair as well as the length of the baseline,
- a dense, raw disparity estimate  $D$  for  $\mathbf{R}$  of the same resolution as  $\mathbf{R}$ , and
- a set  $M$  comprising the pixels where the value of  $D$  is missing.

These requirements can be easily fulfilled with a stereo camera and a standard stereo matching algorithm [30].

The main steps of our pipeline are the following:

1. calculation of a raw depth map  $d$  in meters,
2. *denoising and completion* of  $d$  to produce a refined depth map  $d'$  in meters,
3. calculation of a scene distance map  $\ell$  in meters from  $d'$ ,
4. application of (2) to obtain an initial transmission map  $\hat{t}$ , and
5. guided filtering [28] of  $\hat{t}$  using  $\mathbf{R}$  as guidance to compute the final transmission map  $t$ .

The central idea is to leverage the accurate structure that is present in the color images of the stereo pair in order to improve the quality of depth, before using the latter as input for computing transmission. We now proceed in explaining each step in detail. In step 1, we use the input disparity  $D$  in combination with the values of the focal length and the baseline to obtain  $d$ . The missing values for  $D$ , indicated by  $M$ , are also missing in  $d$ .

Step 2 follows a segmentation-based depth filling approach, which builds on the stereoscopic inpainting method presented in [61]. More specifically, we use a superpixel segmentation of the clear image  $\mathbf{R}$  to guide depth denoising and completion at the level of superpixels, making the assumption that each individual superpixel corresponds roughly to a plane in the 3D scene.

First, we apply a photo-consistency check between  $\mathbf{R}$  and  $\mathbf{Q}$ , using the input disparity  $D$  to establish pixel

correspondences between the two images of the stereo pair, similar to Equation (12) in [61]. All pixels in  $\mathbf{R}$  for which the color deviation (measured as difference in the RGB color space) from the corresponding pixel in  $\mathbf{Q}$  has greater magnitude than  $\epsilon = 12/255$  are deemed invalid regarding depth and hence are added to  $M$ .

We then segment  $\mathbf{R}$  into superpixels with SLIC [2], denoting the target number of superpixels as  $\hat{K}$  and the relevant range domain scale parameter as  $m = 10$ . For depth denoising and completion on Cityscapes, we use  $\hat{K} = 2048$ . The final number of superpixels that are output by SLIC is denoted by  $K$ . These superpixels are classified into reliable and unreliable ones with respect to depth information, based on the number of pixels with missing or invalid depth that they contain. More formally, we use the criterion of Equation (2) in [61], which states that a superpixel  $T$  is reliable if and only if

$$\text{card}(T \setminus M) \geq \max\{P, \lambda \text{card}(T)\}, \quad (4)$$

setting  $P = 20$  and  $\lambda = 0.6$ .

For each superpixel that fulfills (4), we fit a depth plane by running RANSAC on its pixels that have a valid value for depth. We use an adaptive inlier threshold to account for differences in the range of depth values between distinct superpixels. For a superpixel  $T$ , the inlier threshold is set as

$$\theta = 0.01 \text{ median}_{\mathbf{x} \in T \setminus M} \{d(\mathbf{x})\}. \quad (5)$$

We use adaptive RANSAC and set the maximum number of iterations to 2000 and the bound on the probability of having obtained a pure inlier sample to  $p = 0.99$ .

The greedy approach of [61] is used subsequently to match unreliable superpixels to reliable ones pairwise and assign the fitted depth planes of the latter to the former. Different than [61], we propose a novel objective function for matching pairs of superpixels. For a superpixel pair  $(s, t)$ , our proposed objective is formulated as

$$E(s, t) = \|\mathbf{C}_s - \mathbf{C}_t\|^2 + \alpha \|\mathbf{x}_s - \mathbf{x}_t\|^2. \quad (6)$$

The first term measures the proximity of the two superpixels in the range domain, where we denote the average CIELAB color of superpixel  $s$  with  $\mathbf{C}_s$ . In other words, we penalize the squared Euclidean distance between the average colors of the superpixels in the CIELAB color space, which has been designed to increase perceptual uniformity [13]. On the contrary, the objective of [61] uses the cosine similarity of average superpixel colors to form the range domain cost:

$$1 - \frac{\mathbf{C}_s}{\|\mathbf{C}_s\|} \cdot \frac{\mathbf{C}_t}{\|\mathbf{C}_t\|}. \quad (7)$$

The disadvantage of (7) is that it assigns zero matching cost to dissimilar colors in certain cases. For instance, in the RGB color space, the pair of colors  $(\delta, \delta, \delta)$  and  $(1 - \delta, 1 - \delta, 1 - \delta)$ , where  $\delta$  is a small positive constant, is assigned zero penalty, even though the former color is very dark gray and the latter is very light gray.

The second term on the right-hand side of (6) measures the proximity of the two superpixels in the spatial domain as the squared Euclidean distance between their centroids  $\mathbf{x}_s$  and  $\mathbf{x}_t$ . By contrast, the spatial proximity term of [61] assigns zero cost to pairs of adjacent superpixels and unit cost to non-adjacent pairs. This implies that close yet non-adjacent superpixels are penalized equally to very distant superpixels by [61]. As a result, a certain superpixel  $s$  can be erroneously matched to a very distant superpixel  $t$  which is highly unlikely to share the same depth plane as  $s$ , as long as the range domain term for this pair is minimal and all superpixels adjacent to  $s$  are dissimilar to it with respect to appearance. Our proposed spatial cost handles these cases successfully:  $t$  is assigned a very large spatial cost for being matched to  $s$ , and other superpixels that have less similar appearance yet smaller distance to  $s$  are preferred.

In (6),  $\alpha > 0$  is a parameter that weights the relative importance of the spatial domain term versus the range domain term. Similarly to [2], we set  $\alpha = m^2/S^2$ , where  $S = \sqrt{N/K}$  and  $N$  denotes the total number of pixels in the image. Our matching objective (6) is similar to the distance that is defined in SLIC [2] and other superpixel segmentation methods for assigning *an individual pixel to a superpixel*. In our case though, this distance is rather used to measure similarity between *pairs of superpixels*.

After all superpixels have been assigned a depth plane, we use these planes to complete the missing depth values for pixels belonging to  $M$ . In addition, we replace the depth values of pixels which do not belong to  $M$  but constitute large-margin outliers with respect to their corresponding plane (deviation larger than  $\hat{\theta} = 50\text{m}$ ) with the values imputed by the plane. This results in a complete, denoised depth map  $d'$ , and concludes step 2.

In step 3, we compute the distance  $\ell(\mathbf{x})$  of the scene from the camera at each pixel  $\mathbf{x}$  based on  $d'(\mathbf{x})$ , using the coordinates of the principal point plus the focal length of the camera.

Finally, in step 5 we post-process the initial transmission map  $\hat{t}$  with guided filtering [28], in order to smooth transmission while respecting the boundaries of the clear image  $\mathbf{R}$ . We fix the radius of the guided filter window to  $r = 20$  and the regularization param-

eter to  $\mu = 10^{-3}$ , *i. e.* we use the same values as in the haze removal experiments of [28].

Results of the presented pipeline for fog simulation on example images from Cityscapes are provided in Figure 2 for  $\beta = 0.01$ , which corresponds to visibility of ca. 400m. We compare our fog simulation against an alternative implementation, which employs nearest-neighbor interpolation to complete the missing values of the depth map before computing the transmission and does not involve guided filtering as a postprocessing step.

### 3.3 Input Selection for High-Quality Fog Simulation

Applying the presented pipeline to simulate fog on a large dataset with real outdoor scenes such as Cityscapes with the aim of producing synthetic foggy images of high quality calls for careful refinement of the input.

To be more precise, the sky is clear in the majority of scenes in Cityscapes, with intense direct or indirect sunlight, as shown in Figure 3(a). These images usually contain sharp shadows and have high contrast compared to images that depict foggy scenes. This causes our fog simulation to generate synthetic images which do not resemble real fog very well, *e. g.* Figure 3(b). Therefore, our first refinement criterion is whether the sky is overcast, ensuring that the light in the input real scene is not strongly directional.

Secondly, we observe that atmospheric light estimation in step 2 of our fog simulation sometimes fails to select a pixel with ground truth semantic label *sky* as the representative of the value of atmospheric light. In rare cases, it even happens that the sky is not visible at all in an image. This results in an erroneous, physically invalid value of atmospheric light being used in (1) to synthesize the foggy image. Consequently, our second refinement criterion is whether the pixel that is selected as atmospheric light is labeled as *sky*, and affords an automatic implementation.

## 4 Foggy Datasets

We present two distinct datasets for semantic understanding of foggy scenes: *Foggy Cityscapes* and *Foggy Driving*. The former derives from the Cityscapes dataset [14] and constitutes a collection of synthetic foggy images generated with our proposed fog simulation that automatically inherit the semantic annotations of their real, clear counterparts. On the other hand, *Foggy Driving* is a collection of 101 real-world



**Fig. 2** Comparison of our fog simulation to nearest-neighbor interpolation for depth completion on images from Cityscapes. This figure is better seen on a screen and zoomed in

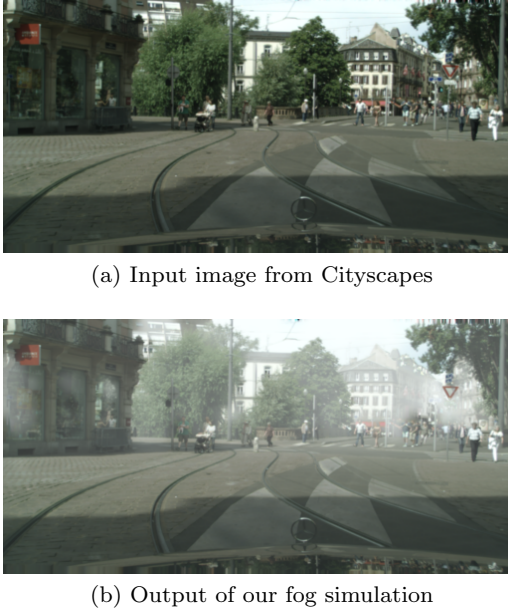


**Fig. 3** Sunny scene from Cityscapes along with the result of our fog simulation

foggy road scenes with annotations for semantic segmentation and object detection, used as a benchmark for the domain of foggy weather.

#### 4.1 Foggy Cityscapes

We apply the fog simulation pipeline that is presented in Section 3 to the complete set of images provided in the Cityscapes dataset. More specifically, we first obtain 20000 synthetic foggy images from the larger, coarsely annotated part of the dataset, and keep all of

them, without applying the refinement criteria of Section 3.3. In this way, we trade the high visual quality of the synthetic images for a very large scale and variability of the synthetic dataset. We do not make use of the original coarse annotations of these images for semantic segmentation; rather, we produce labellings with state-of-the-art semantic segmentation models on the original, clear images and use them as weak supervision, as will be discussed in Section 6. We name this set *Foggy Cityscapes-coarse*.

In addition, we use the two criteria of Section 3.3 in conjunction to filter the finely annotated part of Cityscapes that originally comprises 2975 training and 500 validation images, and obtain a refined set of 550 images, 498 from the training set and 52 from the validation set, which fulfill both criteria. Running our fog simulation on this refined set provides us with a collection of high-quality synthetic foggy images with a moderate scale. This collection automatically inherits the original fine annotations for *semantic segmentation*, as well as bounding box annotations for *object detection* which we generate by leveraging the instance-level semantic annotations that are provided in Cityscapes for the 8 classes *person*, *rider*, *car*, *truck*, *bus*, *train*, *motorcycle* and *bicycle*. We term this collection *Foggy Cityscapes-refined*.

Since MOR can vary significantly in reality for different instances of fog, we generate three distinct variants of *Foggy Cityscapes*, each of which is characterized by a constant simulated attenuation coefficient  $\beta$  in (2), hence a constant MOR. In particular, we use  $\beta \in \{0.005, 0.01, 0.02\}$ , which correspond approximately to MOR of 800m, 400m and 200m respectively.

Figure 4 shows the synthesized fog of the three densities for a scene.

## 4.2 Foggy Driving

*Foggy Driving* consists of 101 color images depicting real-world foggy driving scenes. We captured 51 of these images with a cell phone camera in foggy conditions at various areas of Zurich, and the rest 50 images were carefully collected from the web. We note that all images have been preprocessed so that they have a maximum resolution of  $960 \times 1280$  pixels.

We provide dense, pixel-level semantic annotations for all images of *Foggy Driving*. In particular, we use the 19 evaluation classes of Cityscapes: *road, sidewalk, building, wall, fence, pole, traffic light, traffic sign, vegetation, terrain, sky, person, rider, car, truck, bus, train, motorcycle* and *bicycle*. Pixels that do not belong to any of the above classes or are not labeled are assigned the *void* label, and they are ignored for semantic segmentation evaluation. At annotation time, we label individual instances of *person, rider, car, truck, bus, train, motorcycle* and *bicycle* separately following the Cityscapes annotation protocol, which directly affords bounding box annotations for these 8 classes.

In total, 33 images have been finely annotated (c.f. the last three rows of Figure 12) in the aforementioned procedure, and the rest 68 images have been coarsely annotated (c.f. the top three rows of Figure 12). We provide per-class statistics for the pixel-level semantic annotations of *Foggy Driving* in Figure 5. Furthermore, statistics for the number of objects in the bounding box annotations are shown in Figure 6. Because of the coarse annotation that is created for one part of *Foggy Driving*, we do not use this part in evaluation of object detection approaches, as difficult objects that are not included in the annotations may be detected by a good method and missed by a comparatively worse method, resulting in incorrect comparisons with respect to precision. On the contrary, the coarsely annotated images are used without such issues in evaluation of semantic segmentation approaches, since predictions at unlabeled pixels are simply ignored and thus do not affect the measured performance.

*Foggy Driving* may have a smaller size than other recent datasets for semantic scene understanding, however, it features challenging foggy scenes with comparatively high complexity. As Table 1 shows, the subset of 33 images with fine annotations is roughly on par with Cityscapes regarding the average number of humans and vehicles per image. In total, *Foggy Driving* contains more than 500 vehicles and almost 300 humans. We also

**Table 1** Absolute and average number of annotated pixels, humans and vehicles for Foggy Driving (“Ours”), KITTI and Cityscapes. Only the training and validation sets of KITTI and Cityscapes are considered

	pixels	humans	vehicles	h/im	v/im
Ours (fine)	38.3M	236	288	<b>7.2</b>	8.7
Ours (coarse)	34.6M	54	221	0.8	3.3
KITTI	0.23G	6.1k	30.3k	0.8	4.1
Cityscapes	<b>9.43G</b>	<b>24.0k</b>	<b>41.0k</b>	7.0	<b>11.8</b>

underline the fact that Table 1 compares *Foggy Driving* — a dataset used purely for testing — against the unions of training and validation sets of KITTI [22] and Cityscapes, which are much larger than their respective testing sets that would provide a better comparison.

As a final note, we identify the subset of the 19 annotated classes that occur frequently in *Foggy Driving*. These “frequent” classes either have a larger number of total annotated pixels, *e. g.* *road*, or a larger number of total annotated polygons or instances, *e. g.* *pole* and *person*, compared to the rest of the classes. They are: *road, sidewalk, building, pole, traffic light, traffic sign, vegetation, sky, person*, and *car*. In the experiments that follow in Section 5.1, we occasionally use this set of frequent semantic classes as an alternative to the complete set of semantic classes for averaging per-class scores, in order to further verify the respective result with another result that is based only on classes with plenty of examples.

## 5 Supervised Learning with Synthetic Fog

We first show that our synthetic *Foggy Cityscapes-refined* dataset can be used per se for successfully adapting modern CNN models to the condition of fog with the usual supervised learning paradigm. Our experiments focus primarily on the task of semantic segmentation and additionally include comparisons on the task of object detection, evidencing clearly the usefulness of our synthetic foggy data in understanding the semantics of real foggy scenes.

More specifically, the general outline of our experiments can be summarized in two steps:

1. fine-tuning a model that has been trained on the original Cityscapes dataset for clear weather by using only synthetic images of *Foggy Cityscapes-refined*, and
2. evaluating the fine-tuned model on *Foggy Driving* and comparing its performance against the original model.

In other words, all models are ultimately evaluated on data from a different domain than that of the data on



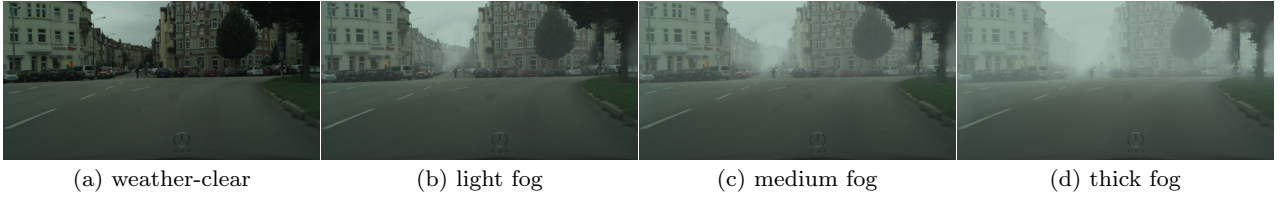


Fig. 4 Exemplar images in *Foggy Cityscapes* with varying fog thickness.

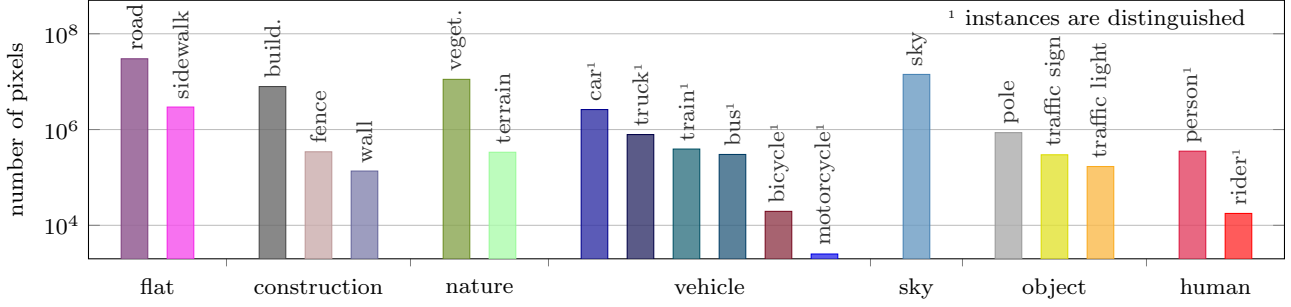


Fig. 5 Number of annotated pixels per class for Foggy Driving

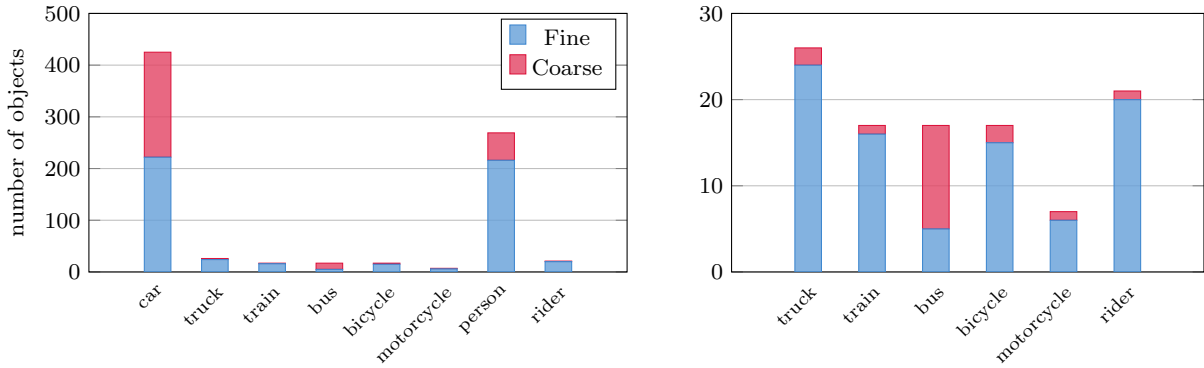


Fig. 6 Number of objects per class in Foggy Driving

which they have been fitted, revealing their true generalization potential on previously unseen foggy scenes.

We also examine the effect of dehazing on performance of semantic segmentation models, employing state-of-the-art dehazing methods in our experiments.

### 5.1 Semantic Segmentation

Our model of choice for conducting experiments on semantic segmentation with the supervised pipeline is the modern dilated convolutions network (DCN) [63]. In particular, we make use of the publicly available *Dilation10* model, which has been trained on the 2975 images of the training set of Cityscapes. We wish to note that this model was originally trained and tested on  $1396 \times 1396$  image crops by the authors of [63], but due to GPU memory limitations we train it on  $756 \times 756$  crops and test it on  $700 \times 700$  crops. Still, *Dilation10*

enjoys a fair mean intersection over union (IoU) score of 34.9% on *Foggy Driving*.

In the following experiments, we fine-tune *Dilation10* on the training set of *Foggy Cityscapes-refined* which consists of 498 images, and reserve the 52 images of the respective validation set for additional evaluation. In particular, we fine-tune all layers of the original model for 3k iterations (ca. 6 epochs) using mini-batches of size 1. Unless otherwise mentioned, the attenuation coefficient  $\beta$  used in *Foggy Cityscapes* is equal to 0.01.

**Comparison of Fog Simulation Approaches.** First, we compare in Table 2 our proposed method for fog simulation on Cityscapes in terms of semantic segmentation performance on *Foggy Driving* against two alternative approaches: the baseline that we considered in Figure 2 and a truncated version of our method, where we omit the guided filtering step. We consider two dif-

**Table 2** Comparison of our fog simulation against two baselines, using different learning rate policies when fine-tuning the segmentation model. Mean IoU (%) over *all* classes is used to report results

	Constant l.r.	“Poly” l.r.
Nearest neighbor	32.9	36.2
Ours w/o guided filtering	33.0	36.8
Ours	<b>34.4</b>	<b>37.8</b>

ferent policies for the learning rate when fine-tuning: a constant learning rate of  $10^{-5}$  and a polynomially decaying learning rate, commonly referred to as “poly”, with a base learning rate of  $10^{-5}$  and a power parameter of 0.9. Our method for fog simulation consistently outperforms the two baselines and the “poly” learning rate policy allows the model to be fine-tuned more effectively than the constant policy. In the rest of our experiments with DCN, we use the “poly” learning rate policy with the parameters specified above for fine-tuning.

**Benefit of Fine-tuning on Synthetic Fog.** The next experiment investigates the benefit of fine-tuning on *Foggy Cityscapes-refined* in improving semantic segmentation performance on *Foggy Driving*. We consider four different options regarding dehazing: applying no dehazing at all, dehazing with multi-scale convolutional neural networks (MSCNN) [47], dehazing using the dark channel prior (DCP) [27], and non-local image dehazing [5]. In all cases, we first apply dehazing (if necessary) on the synthetic foggy images of *Foggy Cityscapes-refined* and then use the (optionally) dehazed images to fine-tune *Dilation10*. At evaluation time, we test each model on *Foggy Driving* after having applied the same dehazing step as the one that was used at training time. Results are provided in Table 3 for all annotated classes in *Foggy Driving* and Table 4 for frequent classes only. Indeed, all fine-tuned models outperform *Dilation10* irrespective of which dehazing approach (if any) is applied, both for mean IoU over all classes and over frequent classes only. The best-performing fine-tuned model, which we refer to as *FT-0.01*, involves no dehazing and outperforms *Dilation10* significantly, giving a relative improvement of almost 10% for both measures. Note additionally that *FT-0.01* has been fine-tuned on only 498 training images of *Foggy Cityscapes-refined*, compared to the 2975 training images of Cityscapes for *Dilation10*.

**Increasing Returns at Larger Distance.** As can easily be deduced from (2), fog has a growing effect on the appearance of the scene as distance from the camera increases. Ideally, a model that is dedicated to foggy scenes must deliver a greater benefit for distant parts of the scene. In order to examine this aspect of

**Table 3** Comparison of *Dilation10* versus fine-tuned versions of it on *Foggy Cityscapes-refined*, for four different options as far as dehazing is concerned. “FT” stands for using fine-tuning and “W/o FT” for not using fine-tuning. Mean IoU (%) over *all* classes is used to report results

	No dehazing	MSCNN	DCP	Non-local
W/o FT	34.9	34.7	29.9	29.3
FT	<b>37.8</b>	<b>37.1</b>	<b>37.4</b>	<b>36.6</b>

**Table 4** Comparison of *Dilation10* versus fine-tuned versions of it on *Foggy Cityscapes-refined*, for four different options as far as dehazing is concerned. “FT” stands for using fine-tuning and “W/o FT” for not using fine-tuning. Mean IoU (%) over *frequent* classes in *Foggy Driving* is used to report results

	No dehazing	MSCNN	DCP	Non-local
W/o FT	52.4	52.4	45.5	46.2
FT	<b>57.4</b>	<b>56.2</b>	<b>56.7</b>	<b>55.1</b>

semantic segmentation of foggy scenes, we use the completed, dense distance maps of Cityscapes images that have been computed as an intermediate output of our fog simulation, given that *Foggy Driving* does not include depth information. In more detail, we consider the validation set of *Foggy Cityscapes-refined*, the images of which are unseen both for *Dilation10* and our fine-tuned models, and bin the pixels according to their value in the corresponding distance map. Each distance range is considered separately for evaluation by ignoring all pixels that do not belong to it. In Figure 7, we compare mean IoU of *Dilation10* and *FT-0.01* individually for each distance range. *FT-0.01* brings a consistent gain in performance across all distance ranges. What is more, this gain is larger in both absolute and relative terms for pixels that are more than 50m away from the camera, implying that our model is able to handle better the most challenging parts of a foggy scene. Note that most pixels in the very last distance range (more than 400m away from the camera) belong to the *sky* class and their appearance does not change much between the clear and the synthetic foggy images.

**Training on Varying Levels of Synthetic Fog.** Our final experiment on semantic segmentation considers three different versions of *Foggy Cityscapes-refined* for fine-tuning *Dilation10*, which correspond to three different values of attenuation coefficient  $\beta$ , as described in Section 4.1. Again, we use the same protocol regarding dehazing and measure the mean IoU performance of the 12 resulting models on *Foggy Driving* for all classes in Table 5 and frequent classes in Table 6.

The two goals that have to be met in order for these models to achieve better performance are:

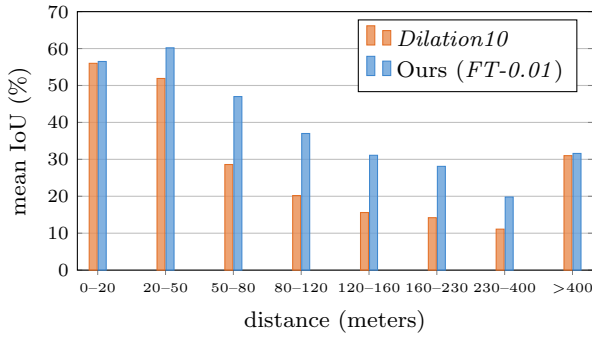


**Fig. 7** Performance of semantic segmentation models on *Foggy Cityscapes-refined* at distinct ranges of scene distance from the camera

**Table 5** Comparison of fine-tuned versions of *Dilation10* on *Foggy Cityscapes-refined*, for three different values of attenuation coefficient  $\beta$  in fog simulation and four different options with regard to dehazing. Mean IoU (%) over *all* classes is used to report results

	$\beta = 0.005$	$\beta = 0.01$	$\beta = 0.02$
No dehazing	37.6	37.8	36.1
MSCNN	<b>38.3</b>	37.1	36.9
DCP	36.6	37.4	36.1
Non-local	36.2	36.6	35.3

**Table 6** Comparison of fine-tuned versions of *Dilation10* on *Foggy Cityscapes-refined*, for three different values of attenuation coefficient  $\beta$  in fog simulation and four different options with regard to dehazing. Mean IoU (%) over *frequent* classes in *Foggy Driving* is used to report results

	$\beta = 0.005$	$\beta = 0.01$	$\beta = 0.02$
No dehazing	57.0	<b>57.4</b>	56.2
MSCNN	57.3	56.2	56.3
DCP	56.0	56.7	55.2
Non-local	55.1	55.1	54.5

1. a good matching in the distributions of the synthetic training data and the real, testing data, and
2. a clear appearance of both sets of data, in the sense that the segmentation model has an easy job in minimizing discriminative features from the data.

Focusing on the case that does not involve dehazing, it is clear from [Table 5](#) and [Table 6](#) that our synthetic images of *Foggy Cityscapes* match better with images of *Foggy Driving* when lower values of  $\beta$  are used, *i. e.* for light or medium fog.

On the other hand, each of the three dehazing methods that are examined has its own particularities in enhancing the appearance of foggy scenes while also introducing artifacts to the output. More specifically, MSCNN operates better at lighter fog, providing a significant improvement with regard to point 2 in this condition. Combined with our conclusion in the previous

paragraph, this explains why MSCNN combined with fine-tuning on light fog ( $\beta = 0.005$ ) delivers one of the two best overall results.

By contrast, DCP is known to operate better at high levels of haze or fog, as its estimated transmission is biased towards lower values [56]. Consequently, DCP is not at its optimal operation point on *Foggy Driving*, as it degrades the quality of images with light fog. Even though it performs better on images with heavy fog than the other two approaches, these images are harder for the segmentation model to identify good features. For this reason, the performance of models that are fine-tuned on images dehazed with DCP peaks at medium rather than light fog, but it is still lower compared to the best MSCNN-based model. Additionally, non-local image dehazing uses a different model for estimating atmospheric light than the one that is shared by our fog simulation, MSCNN and DCP, which implies that it already faces greater difficulty in dehazing images from *Foggy Cityscapes* that are fed to the fine-tuning step, and thus exhibits lower performance.

## 5.2 Evaluation of Image Dehazing Methods

### 5.2.1 Effect on Semantic Segmentation

In [Section 5](#), we observe that providing dehazed images from *Foggy Cityscapes-refined* as intermediate results to the fine-tuning step does not result in a performance gain for SFSU. This can largely be ascribed to two reasons.

First, most of the popular dehazing approaches, including the three approaches that are examined here, rely on the optical model (1) for removing haze or fog. This model assumes a linear relation between the number of incident photons at a pixel and the actual value of the pixel in the processed hazy image. Therefore, these dehazing approaches require that an initial gamma correction step be applied to the pixel intensities before the image is dehazed, otherwise their performance may deteriorate significantly. This in turn implies that the value of gamma is known for each image, which is *not* the case for *Cityscapes* and *Foggy Driving*. Manually searching for the “best” value individually for each image is also infeasible for these large datasets. As a consequence, in the absence of any further information, we have used a constant value of 1 for gamma as the authors of [5] recommend in the implementation of their method, which is probably suboptimal for a large percentage of the images and apparently affects the measured performance for semantic segmentation. We thus wish to point out that future work on outdoor datasets, whether considering fog/haze or not, should ideally record the value of gamma for each image, so

that dehazing methods can show their full potential on the original or derivative, synthetic images of such datasets.

Second, in the real-world scenario of *Foggy Driving*, the homogeneity and uniformity assumptions of the optical model (1) that is used by all examined dehazing methods may not hold exactly. Of course, the same model is used in our fog simulation, however, foggy image synthesis is a *forward* problem, whereas image defogging/dehazing is an *inverse* problem, hence inherently more difficult. As a result, the similarity of synthetic foggy images of *Foggy Cityscapes* to real foggy images of *Foggy Driving* is apparently greater than the similarity of dehazed images from *Foggy Cityscapes* to dehazed images from *Foggy Driving*. This fact appears to compensate the slight increase in visibility for dehazed images in terms of performance of fine-tuned DCN models.

To better understanding the effect of image dehazing, we investigate how much image dehazing increases the visibility of foggy images in our datasets, and how this correlates with the its usefulness for SFSU.

### 5.2.2 Assessing the Visual Quality of Dehazed Images

In order to provide a more complete picture of the benefit of dehazing, we compare the four aforementioned options with regard to dehazing *individually* on each image of our datasets. Figure 8 presents examples of the tetrads of images that we consider: the foggy image (either from *Foggy Cityscapes-refined* with  $\beta = 0.01$  or *Foggy Driving*) and its dehazed versions using DCP, MSCNN and non-local dehazing. As an objective measure for comparison, we leverage the mean IoU score of the respective fine-tuned segmentation models that are considered in Table 3, measured on each image individually. The classes that do not occur in an image are not considered for computing mean IoU on this image. At the same time, we conduct a survey to acquire subjective comparisons of these four versions and examine whether they agree with the objective ones.

**User Study via Amazon Mechanical Turk.** We aim at comparing the four options for dehazing from an observer’s perspective, more specifically from a driver’s perspective, as our images depict mainly road scenes. Humans are subjective and are not good at giving scores to individual image in a linear scale [35]. We thus follow the literature [50] and choose the paired comparisons technique. The participants are shown two images at a time, side by side, and are asked to simply choose the one for which their view is less disturbed by fog or any artifacts and enables safer driving. We use Amazon Mechanical Turk (AMTurk) for the annotation.

We have performed the paired comparison over both *Foggy Cityscapes-refined* and *Foggy Driving*. In total, we obtain  $\binom{4}{2}=6$  per image  $\times 651 = 3906$  comparisons. The annotators are asked to perform five paired comparisons in each of the Human Intelligence Tasks (HITs). Each HIT posted to AMTurk has been completed by three independent Workers for a reliable evaluation. In order to guarantee a good quality for the user study, 1) we have only employed AMTurk Masters for the task, and 2) we verify the answers via a Known Answer Review Policy. Masters are an elite group of Workers, who have demonstrated superior performance while completing thousands of HITs on AMTurk. For the Known Answer Review Policy, we need pairs of images for which the correct answer for the side-by-side comparison is known. To this end, we sample two images of the same scene but with different degrees of fog. In particular, we use images of Cityscapes with clear weather, light fog, and medium fog, leading to  $\binom{3}{2}=3$  per image  $\times 550 = 1650$  pairs. The preference is determined as follows: clear weather is better than light fog, which in turn is better than medium fog. In each HIT, we include five image pairs, of which three are the query pairs and two are pairs with known answers. At an initial step, the left-right order of every image pair is randomly swapped and the order of the five pairs are randomly shuffled, in order to avoid annotations based on memorized patterns.

The overall quality of the user survey is shown in Figure 9, which makes clear that the workers have done a decent job: for 83% of the HITs, both known-answer questions are answered correctly. We only use results from these HITs for our analysis.

**Agreement.** We study first the consistency of choices between annotators; all annotators would be in high agreement if the advantage of one method is obvious and consistent. On the contrast, high disagreement signals difficulty in making choices, suggesting that neither method has dominant advantages. To measure this, we employ the coefficient of agreement [35]:

$$\mu = \frac{2\sigma}{\binom{m}{2}\binom{t}{2}} - 1, \text{ with } \sigma = \sum_{i=1}^t \sum_{j=1}^t \binom{a_{ij}}{2}, \quad (8)$$

where  $a_{ij}$  is the number of times that method  $i$  is chosen over method  $j$ ,  $m = 3$  is the number of annotators for each image, and  $t = 4$  is the number of options with regard to dehazing, including no dehazing. The maximum of  $\mu$  is 1 for complete agreement and the minimum is  $-1/3$  for complete disagreement. The agreement coefficients for all the combinations of image pairs are shown in Table 7. The relatively low values in the table suggest that no single method has dominant advantage over another.



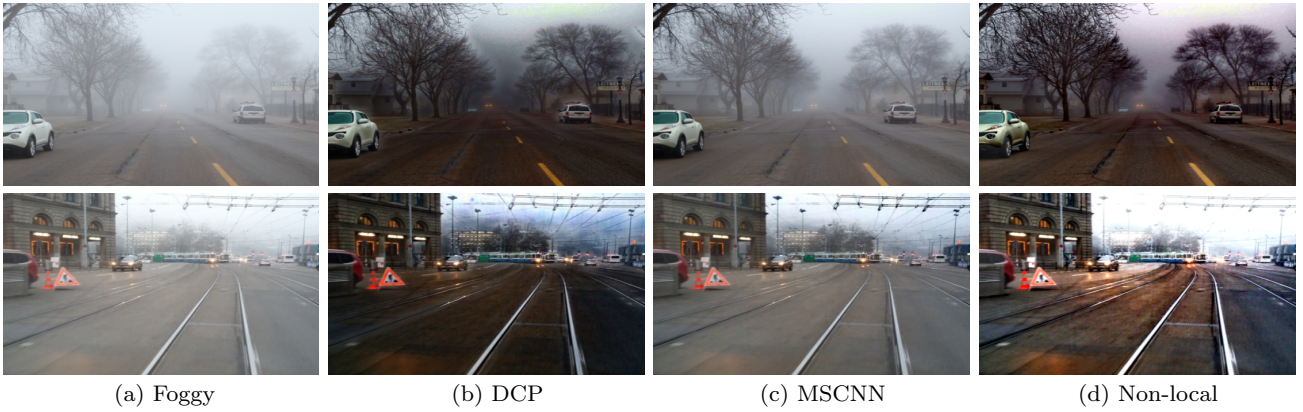


**Fig. 8** Example images from *Foggy Driving* and their dehazed versions using three state-of-the-art dehazing methods that are examined in our experiments

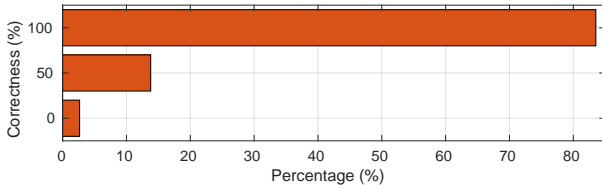


**Fig. 9** Quality of our user survey on AMTurk, computed using known-answer questions

Foggy vs. DCP	0.155
Foggy vs. MSCNN	0.115
Foggy vs. Non-local	0.010
DCP vs. MSCNN	0.182
DCP vs. Non-local	0.036
MSCNN vs. Non-local	0.182
Mean	0.113

**Table 7** Agreement coefficients for all pairwise combinations of the four dehazing options

**Ranking and Correlation.** Figure 10 provides a complete overview of the subjective and objective comparisons of the four examined dehazing options on *Foggy Cityscapes-refined* and *Foggy Driving*. In the middle row of Figure 10, we present the ranking of the four dehazing options with respect to semantic segmentation performance: for each image in the dataset, the option that leads to the highest mean IoU score gets a vote. The rankings that are induced by the results of our survey and the performance of the respective segmentation models for each image are used to compute a correlation score. In this work, we use the *Kendall  $\tau$  distance* [34] to measure the degree of correlation of the two rankings, with  $-1 \leq \tau \leq 1$ , where a value of 1 implies perfect agreement,  $-1$  implies perfect disagreement, and 0 implies zero correlation. In this way, we obtain distributions of  $\tau$  over the entire datasets, which are presented in the bottom row of Figure 10.

Based on the results of Figure 10, it is clear that none of the three examined methods for image dehazing improves reliably the subjective clarity of synthetic foggy images from *Foggy Cityscapes* or real foggy images from *Foggy Driving*, as the foggy versions are ranked first for the largest percentage of images in both datasets. When a large training dataset such as *Foggy Cityscapes* is available, an end-to-end training can adapt the semantic segmentation model very well to the new domain of foggy images. Going to the intermediate results by dehazing methods adds one more layer to the whole pipeline of semantic foggy scene understanding, and thus introduces an additional source of error. This is more pronounced when the dehazing methods indeed do not improve the visual quality for the images of interest.

The dehazing method which is ranked highest in our subjective evaluation is DCP. Moreover, this method is ranked first with respect to objective evaluation in most images of both datasets, beating the model that is fine-tuned on foggy images by a small margin. This result does not contradict the overall mean IoU results for *Foggy Driving* that are reported in Table 3, as the resolution of images in *Foggy Driving* is not constant. We hypothesize that this improvement for DCP when switching from subjective to objective evaluation is partly due to the robustness of CNN architectures, such as DCN, to visual artifacts, allowing the model that is fine-tuned on the dehazed images to place greater importance on the appropriate features. On the other hand, human subjects may be distracted by artifacts introduced by DCP or other dehazing methods (cf. Figure 8), and provide a comparatively lower assessment of the visual clarity of the dehazed image. In addition, as we have previously mentioned in Section 5.1, DCP tends to be more aggressive in removing fog from an image, which helps improve contrast in parts of the

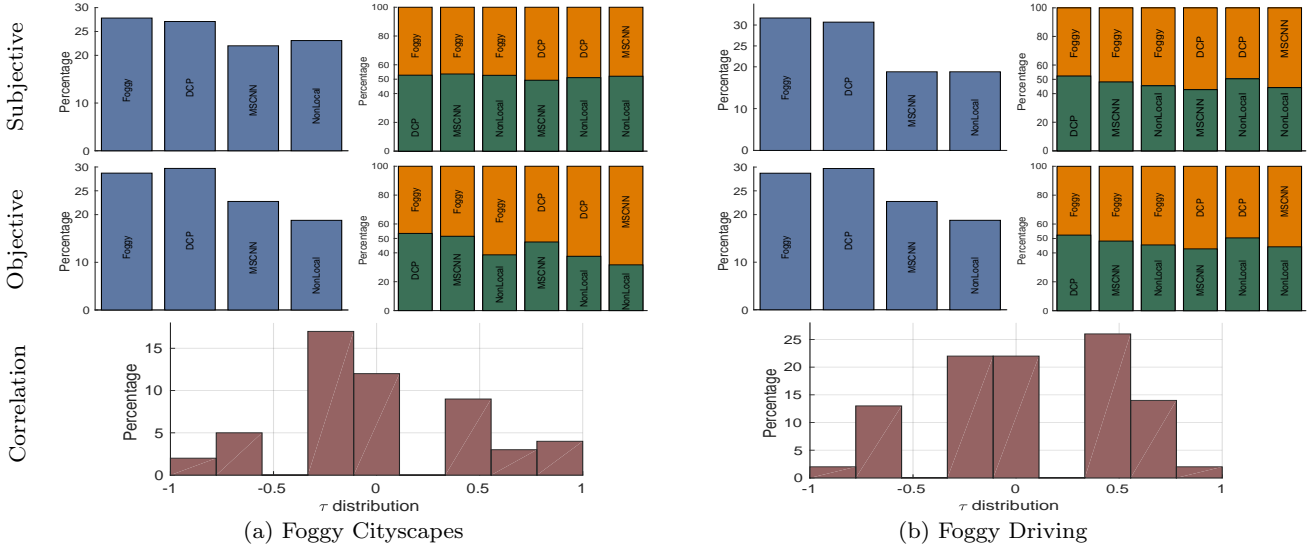


**Fig. 10** Top: Results of our survey on comparing visual quality of foggy images (“Foggy”) and their dehazed versions using “DCP” [27], “MSCNN” [47], and “NonLocal” [5]. We show the percentage of images for which each version is annotated as the best over all versions on the left, and the respective percentages for pairwise comparisons of the four versions on the right. Middle: Similar to top, only that instead of the annotators’ votes we use the objective mean IoU scores of the fine-tuned DCN models that correspond to each of the four versions. For *Foggy Cityscapes-refined*, we restrict our evaluation on the 52 images of the validation set, which have not been presented to the models during training. Bottom: Distribution of the correlation of the four versions’ rankings on each image as measured by the survey and the mean IoU scores, taken over the entire datasets

image which were originally concealed by fog and apparently facilitates semantic segmentation with CNN models to a greater extent. As a final note, our subjective and objective evaluation criteria do exhibit a small positive correlation, based on the left-skewed distributions of the  $\tau$  distance in the bottom row of Figure 10, particularly for the more important, real-world case of *Foggy Driving*.

### 5.3 Object Detection

For our experiment on object detection in foggy scenes, we select the modern Fast R-CNN [23] as the architecture of the evaluated models. We prefer Fast R-CNN over more recent approaches such as Faster R-CNN [46] because the former involves a simpler training pipeline, making fine-tuning to foggy conditions straightforward. Consequently, we do not learn the front-end of the object detection pipeline which involves generation of object proposals; rather, we use multiscale combinatorial grouping [3] for this task.

In order to ensure a fair comparison, we first obtain a baseline Fast R-CNN model for the original Cityscapes dataset, similarly to the preceding semantic segmentation experiments. Since no such model is publicly available, we begin with the model released by the author of [23] which has been trained on PASCAL VOC 2007 [18] and fine-tune it on the union of the

training and validation sets of Cityscapes which comprises 3475 images. Fine-tuning through all layers is run with the same configurations as in [23], except that we use the “poly” learning rate policy with a base learning rate of  $2 \times 10^{-4}$  and a power parameter of 0.9, with 7k iterations (4 epochs).

This baseline model that has been trained on the real Cityscapes with clear weather serves as initialization for fine-tuning on our synthetic images from *Foggy Cityscapes-refined*. To this end, we use all 550 training and validation images of *Foggy Cityscapes-refined* and fine-tune with the same settings as before, only that the base learning rate is set to  $10^{-4}$  and we run 1650 iterations (6 epochs).

We experiment with two values of the attenuation coefficient  $\beta$  for *Foggy Cityscapes-refined* and present comparative performance on the 33 finely annotated images of *Foggy Driving* in Table 8. No dehazing is involved in this experiment. We concentrate on the classes *car* and *person* for evaluation, since they constitute the intersection of the set of frequent classes in *Foggy Driving* and the set of annotated classes with distinct instances. Individual average precision (AP) scores for *car* and *person* are reported, as well as mean scores over these two classes (“mean frequent”) and over the complete set of 8 classes occurring in instances (“mean all”). For completeness, we note that the original VOC 2007 model of [23] exhibits an AP of 2.1% for *car* and 1.9% for *person*.



**Fig. 11** Qualitative results for detection of cars on *Foggy Driving*. From left to right: ground truth annotation, baseline Fast R-CNN model trained on original Cityscapes, and our model *FT-0.005* fine-tuned on *Foggy Cityscapes-refined* with light fog. This figure is seen better when zoomed in on a screen

**Table 8** Comparison of baseline Fast R-CNN model trained on Cityscapes (“W/o FT”) against fine-tuned versions of it on *Foggy Cityscapes-refined*. “FT” stands for using fine-tuning and “W/o FT” for not using fine-tuning. AP (%) is used to report results

	mean all	car	person	mean frequent
W/o FT	11.1	30.5	<b>10.3</b>	20.4
FT $\beta = 0.01$	11.1	34.6	10.0	22.3
FT $\beta = 0.005$	<b>11.7</b>	<b>35.3</b>	<b>10.3</b>	<b>22.8</b>

Both of our fine-tuned models outperform the baseline model by a significant margin for *car*. At the same time, they are on a par with the baseline model for *person*. The overall winner is the model that has been fine-tuned on light fog, which we refer to as *FT-0.005*: it outperforms the baseline model by 2.4% on average

on the two frequent classes and it is also slightly better when taking all 8 classes into account.

We provide a visual comparison of *FT-0.005* and the baseline model for car detection on example images from *Foggy Driving* in Figure 11. Note the ability of our model to detect distant cars, such as the two cars in the image of the second row which are moving on the left side of the road and are visible from their front part. These two cars are both missed by the baseline model.

## 6 Semi-supervised Learning with Synthetic Fog

While standard supervised learning can improve the performance of SFSU using our synthetic fog, the paradigm still needs manual annotations for corresponding weather-clear images. In this section, we extend the learning to a new paradigm which is also able

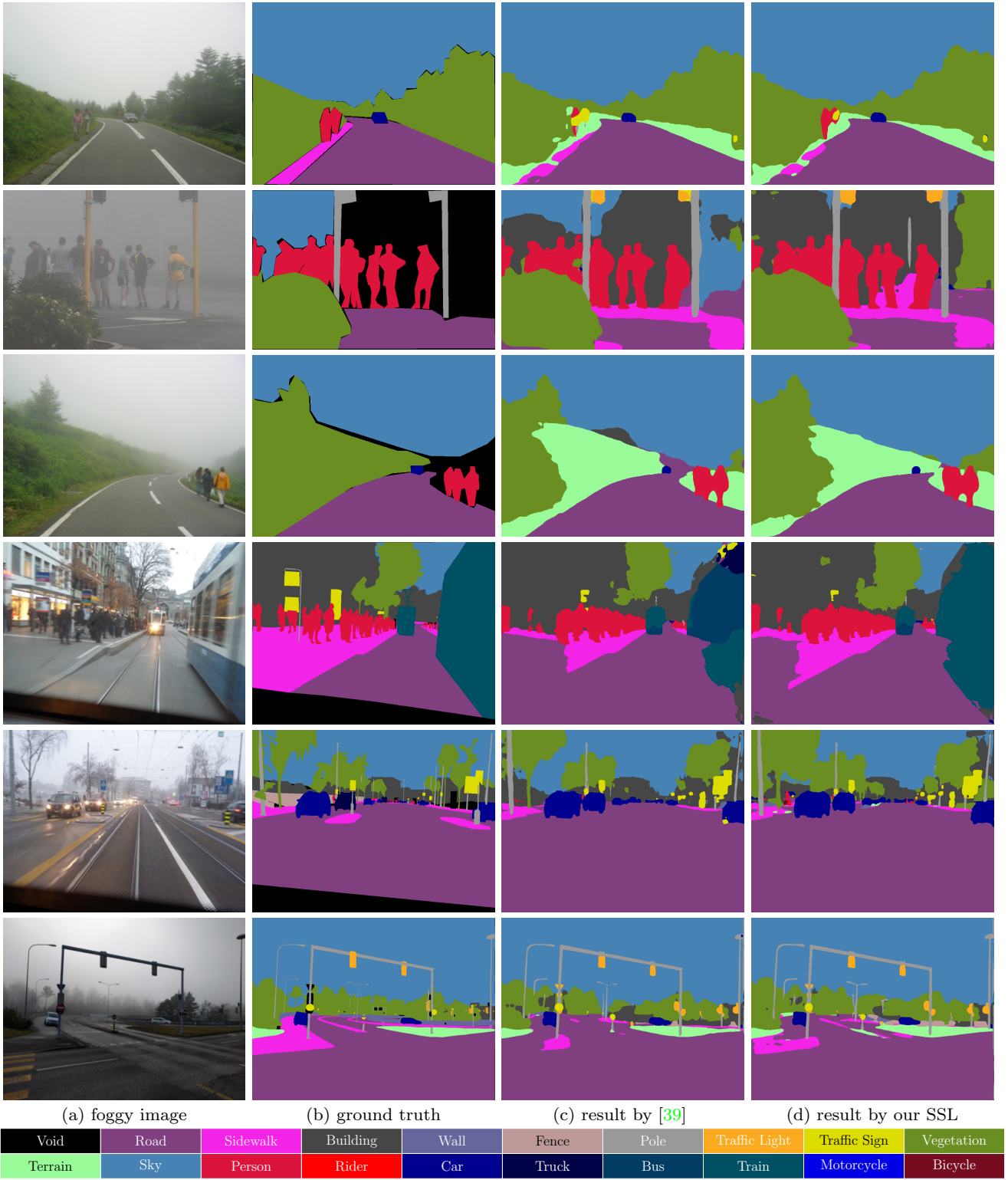


**Fig. 12** Qualitative results for semantic segmentation on *Foggy Driving*, both for coarsely annotated images (top three rows) and finely annotated images (bottom three rows)

to acquire knowledge from unlabeled pairs of foggy images and weather-clear images. In particular, we train a semantic segmentation model on weather-clear im-

ages using the standard supervised learning paradigm, and apply the model to an even larger set of clear but unlabeled images (e.g. our 20000 unlabeled images



of *Foggy Cityscapes-coarse*) to generate the class responses. Since we have created a foggy version for the unlabeled dataset, these class responses can then be used to supervise the training of models for SFSU.

This learning is inspired by the stream of work on model distillation [25, 29] or imitation [10, 15]. [10, 15, 29] transfer supervision from sophisticated models to simpler models for efficiency, and [25] transfers supervision from the domain of images to other domains such as depth maps. In our case, supervision is transferred from clear weather to foggy weather. The underpinnings of our proposed approach are the following: 1) in clear weather, objects are easier to recognize than in foggy weather, thus models trained on images with clear weather in principle generalize better to new images of the same condition than those trained on foggy images; and 2) since the synthetic foggy images and their weather-clear counterparts depict exactly the same scene, recognition results should also be the same for both images ideally.

We formulate the semi-supervised learning (SSL) for semantic segmentation as follows. Let us denote a weather-clear image by  $\mathbf{x}$ , the corresponding foggy one by  $\mathbf{x}'$ , and the corresponding human annotation by  $\mathbf{y}$ . Then, the training data consist of both labeled data  $\mathcal{D}_l = \{(\mathbf{x}_i, \mathbf{x}'_i, \mathbf{y}_i)\}_{i=1}^l$  and unlabeled data  $\mathcal{D}_u = \{(\mathbf{x}_j, \mathbf{x}'_j)\}_{j=l+1}^{l+u}$ , where  $\mathbf{y}_i^{m,n} \in \{1, \dots, K\}$  is the label of pixel  $(m, n)$ , and  $K$  is the total number of classes.  $l$  is the number of labeled training images, and  $u$  is the number of unlabeled training images. The aim is to learn a mapping function  $\phi' : \mathcal{X}' \mapsto \mathcal{Y}$  from  $\mathcal{D}_l$  and  $\mathcal{D}_u$ . For our case,  $\mathcal{D}_l$  consists of the 498 high-quality foggy images in the training set of *Foggy Cityscapes-refined* which have human annotations with fine details, and  $\mathcal{D}_u$  consists of the additional 20000 foggy images in *Foggy Cityscapes-coarse* which do not have fine human annotations.

Since  $\mathcal{D}_u$  does not have class labels, we use the idea of supervision transfer to generate the supervisory labels for all the images therein. To this end, we first learn a mapping function  $\phi : \mathcal{X} \mapsto \mathcal{Y}$  with  $\mathcal{D}_l$  and then obtain the labels  $\hat{\mathbf{y}}_j = \phi(\mathbf{x}_j)$  for  $\mathbf{x}_j$  and  $\mathbf{x}'_j$ ,  $\forall j \in \{l+1, \dots, l+u\}$ .  $\mathcal{D}_u$  is then upgraded to  $\hat{\mathcal{D}}_u = \{(\mathbf{x}_j, \mathbf{x}'_j, \hat{\mathbf{y}}_j)\}_{j=l+1}^{l+u}$ . The proposed scheme for training semantic segmentation models for foggy images  $\mathbf{x}'$  is to learn a mapping function  $\phi'$  so that human annotations  $\mathbf{y}$  and the transferred labels  $\hat{\mathbf{y}}$  are both taken into account:

$$\min_{\phi'} \sum_{i=1}^l L(\phi(\mathbf{x}'_i), \mathbf{y}_i) + \lambda \sum_{j=l+1}^{l+u} L(\phi(\mathbf{x}'_j), \hat{\mathbf{y}}_j), \quad (9)$$

where  $L(., .)$  is the Categorical Cross Entropy Loss function for classification, and  $\lambda = \frac{l}{u} \times w$  is a parameter for

balancing the contribution of the two terms, serving as the relative weight of each unlabeled image compared to each labeled one. We empirically set  $w = 5$  in our experiment, but an optimal value can be obtained via cross-validation if needed. In our implementation, we approximate the optimization of (9) by mixing images from  $\mathcal{D}_l$  and  $\hat{\mathcal{D}}_u$  in a proportion of  $1 : \lambda$  and feeding the stream of hybrid data to a CNN for standard supervised training.

We select Refinenet [39] as the CNN model for semantic segmentation, which is a more recent and better performing method than DCN [63] that is used in Section 5. The reason is that Refinenet had not been published yet at the time that we were conducting the experiments of Section 5. We would like to note that the state-of-the-art PSPNet [65], which has been trained on the Cityscapes dataset similarly to the original version of Refinenet that we use as our baseline, achieved a mean IoU of only 24.0% on *Foggy Driving* in our initial experiments.

We use mean IoU for evaluation, similarly to Section 5. We compare the performance of three trained models: 1) original Refinenet [39] trained on Cityscapes, 2) Refinenet fine-tuned on  $\mathcal{D}_l$ , and 3) Refinenet fine-tuned on  $\mathcal{D}_l$  and  $\hat{\mathcal{D}}_u$ . The mean IoU scores of the three models on *Foggy Driving* are 44.3%, 46.3%, and 49.7% respectively. The 2% improvement of 2) over 1) again confirms the conclusion we draw in Section 5 that fine-tuning with our synthetic fog can indeed improve the performance of semantic foggy scene understanding. The 3.4% improvement of 3) over 2) validates the efficacy of the SSL paradigm. Figure 12 shows visual results of 1) and 3), along with the foggy images and human annotations. The re-trained model with our SSL learning paradigm can better segment certain parts of the images which are misclassified by the original Refinenet. For instance, the pedestrian in the first example, the tram in the fourth one, and the sidewalk in the last one.

Both the quantitative and qualitative results suggest that our approach is able to alleviate the need for collecting large-scale training data for semantic understanding of foggy scenes, by training with the annotations that are already available for weather-clear images and the generated foggy images directly and by transferring supervision from weather-clear images to foggy images of the same scenes.

## 7 Conclusion

In this paper, we have demonstrated the benefit of synthetic data that are based on real images for semantic understanding of foggy scenes. Two foggy datasets

have been constructed to this end: the synthetic *Foggy Cityscapes* dataset which derives from Cityscapes, and the real-world *Foggy Driving* dataset, both with dense pixel-level semantic annotations for 19 classes and bounding box annotations for objects belonging to 8 classes. We have shown that *Foggy Cityscapes* can be used to boost performance of state-of-the-art CNN models for semantic segmentation and object detection on the challenging real foggy scenes of *Foggy Driving*, both in a usual supervised setting and in a novel, semi-supervised setting. Last but not least, we have exposed through detailed experiments the fact that image dehazing faces difficulties in working out of the box on real outdoor foggy data and thus is marginally helpful for SFSU. In the future, we would like to combine dehazing and semantic understanding of foggy scenes into a unified, end-to-end learned pipeline, which can also leverage the type of synthetic foggy data we have introduced.

**Acknowledgements** The authors would like to thank Kevis Maninis for useful discussions. This work is funded by Toyota Motor Europe via the research project TRACE-Zürich.

## References

1. Federal Meteorological Handbook No. 1: Surface Weather Observations and Reports. U.S. Department of Commerce / National Oceanic and Atmospheric Administration (2005)
2. Achanta, R., Shaji, A., Smith, K., Lucchi, A., Fua, P., Sisstrunk, S.: SLIC superpixels compared to state-of-the-art superpixel methods. *IEEE Transactions on Pattern Analysis and Machine Intelligence* **34**(11), 2274–2282 (2012)
3. Arbeláez, P., Pont-Tuset, J., Barron, J., Marques, F., Malik, J.: Multiscale combinatorial grouping. In: *IEEE Conference on Computer Vision and Pattern Recognition (CVPR)* (2014)
4. Bar Hillel, A., Lerner, R., Levi, D., Raz, G.: Recent progress in road and lane detection: A survey. *Mach. Vision Appl.* **25**(3), 727–745 (2014)
5. Berman, D., Treibitz, T., Avidan, S.: Non-local image dehazing. In: *IEEE Conference on Computer Vision and Pattern Recognition (CVPR)* (2016)
6. Bronte, S., Bergasa, L.M., Alcantarilla, P.F.: Fog detection system based on computer vision techniques. In: *International IEEE Conference on Intelligent Transportation Systems* (2009)
7. Bronte, S., Bergasa, L.M., Alcantarilla, P.F.: Fog detection system based on computer vision techniques. In: *International IEEE Conference on Intelligent Transportation Systems*, pp. 1–6 (2009)
8. Brostow, G.J., Shotton, J., Fauqueur, J., Cipolla, R.: Segmentation and recognition using structure from motion point clouds. In: *ECCV*, pp. 44–57 (2008)
9. Buch, N., Velastin, S.A., Orwell, J.: A review of computer vision techniques for the analysis of urban traffic. *IEEE Transactions on Intelligent Transportation Systems* **12**(3), 920–939 (2011)
10. BuciluC, C., Caruana, R., Niculescu-Mizil, A.: Model compression. In: *International Conference on Knowledge Discovery and Data Mining (SIGKDD)* (2006)
11. Camplani, M., Salgado, L.: Efficient spatio-temporal hole filling strategy for Kinect depth maps. In: *Proc. SPIE* (2012)
12. Colomb, M., Hirech, K., André, P., Boreux, J.J., Lacote, P., Dufour, J.: An innovative artificial fog production device improved in the European project “FOG”. *Atmospheric Research* **87**(3), 242–251 (2008)
13. Comaniciu, D., Meer, P.: Mean shift: a robust approach toward feature space analysis. *IEEE Transactions on Pattern Analysis and Machine Intelligence* **24**(5), 603–619 (2002)
14. Cordts, M., Omran, M., Ramos, S., Rehfeld, T., Enzweiler, M., Benenson, R., Franke, U., Roth, S., Schiele, B.: The Cityscapes dataset for semantic urban scene understanding. In: *IEEE Conference on Computer Vision and Pattern Recognition (CVPR)* (2016)
15. Dai, D., Kroeger, T., Timofte, R., Van Gool, L.: Metric imitation by manifold transfer for efficient vision applications. In: *IEEE Conference on Computer Vision and Pattern Recognition (CVPR)* (2015)
16. Dai, D., Yang, W.: Satellite image classification via two-layer sparse coding with biased image representation. *IEEE Geoscience and Remote Sensing Letters* **8**(1), 173–176 (2011)
17. Dosovitskiy, A., Fischery, P., Ilg, E., Häusser, P., Hazirbas, C., Golkov, V., v. d. Smagt, P., Cremers, D., Brox, T.: FlowNet: Learning optical flow with convolutional networks. In: *IEEE International Conference on Computer Vision (ICCV)* (2015)
18. Everingham, M., Van Gool, L., Williams, C.K., Winn, J., Zisserman, A.: The PASCAL visual object classes (VOC) challenge. *IJCV* **88**(2), 303–338 (2010)
19. Fattal, R.: Single image dehazing. *ACM transactions on graphics (TOG)* **27**(3), 72 (2008)
20. Gallen, R., Cord, A., Hautière, N., Aubert, D.: Towards night fog detection through use of in-vehicle multipurpose cameras. In: *IEEE Intelligent Vehicles Symposium (IV)* (2011)
21. Gallen, R., Cord, A., Hautière, N., Dumont, É., Aubert, D.: Nighttime visibility analysis and estimation method in the presence of dense fog. *IEEE Transactions on Intelligent Transportation Systems* **16**(1), 310–320 (2015)
22. Geiger, A., Lenz, P., Urtasun, R.: Are we ready for autonomous driving? The KITTI vision benchmark suite. In: *IEEE Conference on Computer Vision and Pattern Recognition (CVPR)* (2012)
23. Girshick, R.: Fast R-CNN. In: *International Conference on Computer Vision (ICCV)* (2015)
24. Gupta, A., Vedaldi, A., Zisserman, A.: Synthetic data for text localisation in natural images. In: *IEEE Conference on Computer Vision and Pattern Recognition* (2016)
25. Gupta, S., Hoffman, J., Malik, J.: Cross modal distillation for supervision transfer. In: *The IEEE Conference on Computer Vision and Pattern Recognition (CVPR)* (2016)
26. Hautière, N., Tarel, J.P., Lavenant, J., Aubert, D.: Automatic fog detection and estimation of visibility distance through use of an onboard camera. *Machine Vision and Applications* **17**(1), 8–20 (2006)
27. He, K., Sun, J., Tang, X.: Single image haze removal using dark channel prior. *IEEE Transactions on Pattern Analysis and Machine Intelligence* **33**(12), 2341–2353 (2011)
28. He, K., Sun, J., Tang, X.: Guided image filtering. *IEEE Transactions on Pattern Analysis and Machine Intelligence* **35**(6), 1397–1409 (2013)

29. Hinton, G., Vinyals, O., Dean, J.: Distilling the knowledge in a neural network. arXiv preprint arXiv:1503.02531 (2015)
30. Hirschmuller, H.: Stereo processing by semiglobal matching and mutual information. *IEEE Transactions on Pattern Analysis and Machine Intelligence* **30**(2), 328–341 (2008)
31. Janai, J., Güney, F., Behl, A., Geiger, A.: Computer vision for autonomous vehicles: Problems, datasets and state-of-the-art. arXiv preprint arXiv:1704.05519 (2017)
32. Jensen, M.B., Philipsen, M.P., Møgelmoose, A., Moeslund, T.B., Trivedi, M.M.: Vision for looking at traffic lights: Issues, survey, and perspectives. *IEEE Transactions on Intelligent Transportation Systems* **17**(7), 1800–1815 (2016)
33. Johnson-Roberson, M., Barto, C., Mehta, R., Sridhar, S.N., Rosaen, K., Vasudevan, R.: Driving in the matrix: Can virtual worlds replace human-generated annotations for real world tasks? In: *IEEE International Conference on Robotics and Automation* (2017)
34. Kendall, M.G.: A new measure of rank correlation. *Biometrika* **30**(1/2), 81–93 (1938)
35. Kendall, M.G., Smith, B.B.: On the method of paired comparisons. *Biometrika* **31**(3/4), 324–345 (1940)
36. Koschmieder, H.: Theorie der horizontalen Sichtweite. *Beiträge zur Physik der freien Atmosphäre* (1924)
37. Levin, A., Lischinski, D., Weiss, Y.: Colorization using optimization. In: *ACM SIGGRAPH* (2004)
38. Li, Y., Tan, R.T., Brown, M.S.: Nighttime haze removal with glow and multiple light colors. In: *2015 IEEE International Conference on Computer Vision (ICCV)*, pp. 226–234 (2015)
39. Lin, G., Milan, A., Shen, C., Reid, I.: Refinenet: Multi-path refinement networks with identity mappings for high-resolution semantic segmentation. In: *IEEE Conference on Computer Vision and Pattern Recognition (CVPR)* (2017)
40. Miclea, R.C., Silea, I.: Visibility detection in foggy environment. In: *International Conference on Control Systems and Computer Science* (2015)
41. Narasimhan, S.G., Nayar, S.K.: Vision and the atmosphere. *Int. J. Comput. Vision* **48**(3), 233–254 (2002)
42. Narasimhan, S.G., Nayar, S.K.: Contrast restoration of weather degraded images. *IEEE Trans. Pattern Anal. Mach. Intell.* **25**(6), 713–724 (2003)
43. Nishino, K., Kratz, L., Lombardi, S.: Bayesian defogging. *International Journal of Computer Vision* **98**(3), 263–278 (2012)
44. Pavlić, M., Belzner, H., Rigoll, G., Ilić, S.: Image based fog detection in vehicles. In: *2012 IEEE Intelligent Vehicles Symposium* (2012)
45. Pavlić, M., Rigoll, G., Ilić, S.: Classification of images in fog and fog-free scenes for use in vehicles. In: *IEEE Intelligent Vehicles Symposium (IV)* (2013)
46. Ren, S., He, K., Girshick, R., Sun, J.: Faster R-CNN: Towards real-time object detection with region proposal networks. In: *Advances in Neural Information Processing Systems*, pp. 91–99 (2015)
47. Ren, W., Liu, S., Zhang, H., Pan, J., Cao, X., Yang, M.H.: Single image dehazing via multi-scale convolutional neural networks. In: *European Conference on Computer Vision* (2016)
48. Richter, S.R., Vineet, V., Roth, S., Koltun, V.: Playing for data: Ground truth from computer games. In: *European Conference on Computer Vision*, pp. 102–118. Springer (2016)
49. Ros, G., Sellart, L., Materzynska, J., Vazquez, D., Lopez, A.M.: The SYNTHIA dataset: A large collection of synthetic images for semantic segmentation of urban scenes. In: *The IEEE Conference on Computer Vision and Pattern Recognition (CVPR)*, pp. 3234–3243 (2016)
50. Rubinstein, M., Gutierrez, D., Sorkine, O., Shamir, A.: A comparative study of image retargeting. *ACM Trans. Graph.* **29**(6), 160:1–160:10 (2010). DOI 10.1145/1882261.1866186. URL <http://doi.acm.org/10.1145/1882261.1866186>
51. Russakovsky, O., Deng, J., Su, H., Krause, J., Satheesh, S., Ma, S., Huang, Z., Karpathy, A., Khosla, A., Bernstein, M., et al.: Imagenet large scale visual recognition challenge. *International Journal of Computer Vision* **115**(3), 211–252 (2015)
52. Shen, J., Cheung, S.C.S.: Layer depth denoising and completion for structured-light RGB-D cameras. In: *IEEE Conference on Computer Vision and Pattern Recognition (CVPR)* (2013)
53. Silberman, N., Hoiem, D., Kohli, P., Fergus, R.: Indoor segmentation and support inference from RGBD images. In: *ECCV* (2012)
54. Spinneker, R., Koch, C., Park, S.B., Yoon, J.J.: Fast fog detection for camera based advanced driver assistance systems. In: *International IEEE Conference on Intelligent Transportation Systems (ITSC)* (2014)
55. Tan, R.T.: Visibility in bad weather from a single image. In: *IEEE Conference on Computer Vision and Pattern Recognition (CVPR)* (2008)
56. Tang, K., Yang, J., Wang, J.: Investigating haze-relevant features in a learning framework for image dehazing. In: *2014 IEEE Conference on Computer Vision and Pattern Recognition*, pp. 2995–3002 (2014)
57. Tarel, J.P., Hautière, N.: Fast visibility restoration from a single color or gray level image. In: *IEEE International Conference on Computer Vision* (2009)
58. Tarel, J.P., Hautière, N., Caraffa, L., Cord, A., Halmaoui, H., Gruyer, D.: Vision enhancement in homogeneous and heterogeneous fog. *IEEE Intelligent Transportation Systems Magazine* **4**(2), 6–20 (2012)
59. Tarel, J.P., Hautière, N., Cord, A., Gruyer, D., Halmaoui, H.: Improved visibility of road scene images under heterogeneous fog. In: *IEEE Intelligent Vehicles Symposium*, pp. 478–485 (2010)
60. Vázquez, D., Lopez, A.M., Marin, J., Ponsa, D., Geronimo, D.: Virtual and real world adaptation for pedestrian detection. *IEEE Transactions on Pattern Analysis and Machine Intelligence* **36**(4), 797–809 (2014)
61. Wang, L., Jin, H., Yang, R., Gong, M.: Stereoscopic inpainting: Joint color and depth completion from stereo images. In: *IEEE Conference on Computer Vision and Pattern Recognition (CVPR)* (2008)
62. Wang, Y.K., Fan, C.T.: Single image defogging by multiscale depth fusion. *IEEE Transactions on Image Processing* **23**(11), 4826–4837 (2014)
63. Yu, F., Koltun, V.: Multi-scale context aggregation by dilated convolutions. In: *ICLR* (2016)
64. Zhang, J., Cao, Y., Wang, Z.: Nighttime haze removal based on a new imaging model. In: *IEEE International Conference on Image Processing (ICIP)*, pp. 4557–4561 (2014)
65. Zhao, H., Shi, J., Qi, X., Wang, X., Jia, J.: Pyramid scene parsing network. In: *IEEE Conference on Computer Vision and Pattern Recognition (CVPR)* (2017)